ACS NANO

www.acsnano.org

ARTICLE

Octopus-Inspired Assembly of Nanosucker Arrays for Dry/Wet Adhesion

Ying-Chu Chen and Hongta Yang*

Department of Chemical Engineering, National Chung Hsing University, No. 145, Xingda Road, Taichung 40227, Taiwan

Supporting Information

ABSTRACT: **The octopus is capable of adhering to slippery, rough, and irregular surfaces in the marine intertidal zone because of its periodic infundibulum-shaped suckers on the arms. Here, we present a scalable self-assembly technology for fabricating adhesion materials that mimic octopus sucker functionality. By utilizing spin-coated two-dimensional colloidal crystals as templates, non-close-packed nanosucker arrays are patterned on silicone substrates. The resulting nanosuckers can be deformed to exhibit great adhesive capacities on both microrough and flat surfaces in dry and wet environments. This indicates a probable biomimetic solution to the challenge of wound care.**

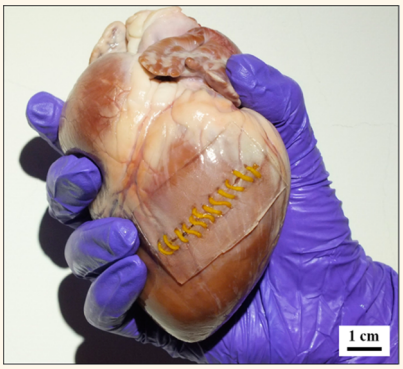

KEYWORDS: *octopus, self-assembly, spin-coating, nanosucker arrays, adhesion*

For long, human beings suffer from wounds, including skin wounds, oral wounds, bleeding wounds, and surgical or traumatic disruption of connective tissue, muscles, tendons, and organs. For emergent bleeding control from open wounds, keeping wounds clean, and achieving wound healing, gauzes have been commonly used.[1,2] Commercial gauzes can be grossly divided into absorbable and nonabsorbable materials; they are easy to produce, preserve, and apply. Nylon is the most widely used nonabsorbable gauze material. Unfortunately, removing the gauze provokes high stress concentration and tends to damage surrounding tissues.[3,4] In addition, the granuloma formation as it resides long on the wound is another issue to be addressed.[5−7] In contrast, absorbable gauze materials, such as poly(lactic-*co*-glycolic acid), often evoke inflammatory reactions and induce undesirable scar formations, including intra-abdominal adhesions.[8−10] Moreover, achieving hemostasis with manual compression through the absorbable or nonabsorbable gauzes can be difficult and time-consuming.

Currently, a variety of hemostatic agents, sealants, and adhesives have been developed to provide easier, faster, and more pragmatic approaches of tissue closure.[11−13] The chemical closure materials work as glues which bind tissues together to progress the natural healing. Nevertheless, the closure materials must be biocompatible, biodegradable, stable, and meet the critical requirements approved by the U.S. Food and Drug Administration (USFDA), and therefore, the types of materials are expensive.[14,15] Furthermore, once the chemicals are applied on wounds, it is required to avoid washing or immersing wounds in water, which may interfere with the healing process.[16,17] Frequently, difficult decisions will arise where closure materials are not easy to remove and where the dose to the underlying tissue may significantly exceed the relevant maximum permissible dose.[18]

Millions of years before people began to create functional structures, natural biological systems developed many architectures to produce functionalities by years of evolution.[19−22] For instance, octopus arms, consisting of non-close-packed centimeter-scale suckers, can attach to objects in order to anchor the octopus body to substratum or manipulate, investigate, grasp, and collect prey.[23] The adhesion is generated by the suckers attaching to a target, forming a seal at the rim, and then inducing a negative pressure in the acetabulum regardless of the target surface materials.[24] Inspired by the adhesion mechanism of octopus suckers, many artificial suckers have been developed to achieve adhesion capabilities for a range of commercial and industrial applications.[25−27] However, the reported octopus-inspired adhesive systems require an additional suctioning system and power sources during the adhesive process to reduce the pressure inside the suction cups.[28−30] Moreover, it is still a challenge to provide a high switching adhesive strength ratio with excellent switchability.[31] Another inherent problem of the adhesion is that the artificial suckers can only be used on a flat target; however, most human body tissues and wounds have bumps, curves, and corners in millimeter/micrometer scale.[32] In addition, in a wet environ-

Received: February 6, 2017
Accepted: April 27, 2017
Published: April 27, 2017

DOI: 10.1021/acsnano.7b00809
ACS Nano 2017, 11, 5332−5338

ment, the friction between the artificial suckers and the wet surface decreases drastically due to fluid lubrication, making the suckers slide under pulling force in the shear direction.[33]

RESULTS AND DISCUSSION

To address the issues, we develop a nanosucker array using a scalable spin-coating technology, which enables large-scale fabrication of non-close-packed colloidal crystals.[34−36] This bottom-up self-assembly methodology is realized by shear-aligning concentrated silica colloidal suspensions with 20% silica particle fraction.[37] Figure 1a displays the photo of a monolayer 250 nm silica colloidal crystal/ethoxylated trimethylolpropane triacrylate (ETPTA) polymer composite spin-coated on a 4 in. diameter silicon wafer. Under white light illumination, the wafer exhibits distinctive six-arm Bragg diffraction patterns, indicating long-range hexagonal ordering and the non-close-packed structure of colloidal crystal, which is identical to the appearance of spin-coated silica colloidal crystals on silicon wafers.[38] The crystal lattice structure is further demonstrated by the side-view SEM image, as shown in Figure 1b. Although some defects, which are mostly caused by silica particles with distinct sizes, are apparent, the long-range hexagonal arrangement of silica particles is clearly observed from the SEM image. Additionally, a thin ETPTA polymer wetting layer separating the silica particles from the silicon wafer surface is evident.

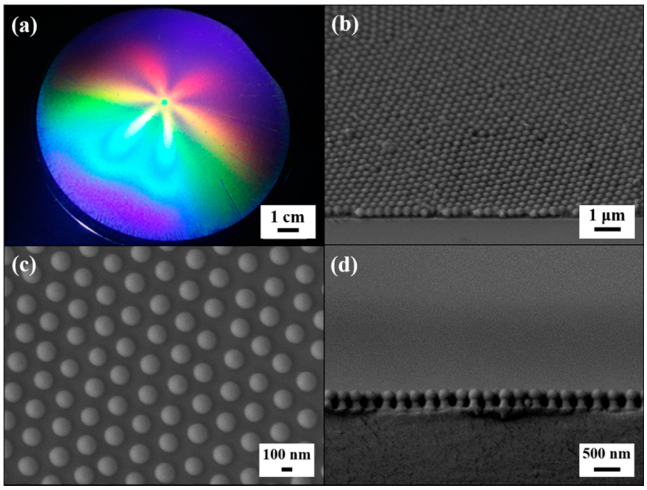

Figure 1. Non-close-packed silica colloidal crystal on a silicon wafer fabricated by the spin-coating technology. (a) Photograph of a sample illuminated with white light. (b) Side-view SEM image. (c) Top-view and (d) cross-sectional SEM images of a periodic array of mushroom-like structures consisting of silica spherical caps and ETPTA polymer stems on the silicon wafer prepared by plasma etching.

The ETPTA polymer matrix can then be partially removed by performing an oxygen/argon reactive ion etching (RIE) treatment. Because the etching rate of the ETPTA polymer is much higher than that of silica, the silica particles are capable of functioning as etching masks during the RIE process and protecting the ETPTA wetting layer immediately underneath them from being etched. The residual polymer matrix maintains sufficient mechanical robustness of the released silica particles, leading to the formation of mushroom-like features, which consists of top silica caps and bottom ETPTA polymer stems. In Figure 1c, the hexagonal ordering and non-close-packed arrangement of nanomushrooms are clearly evident from the top-view SEM image. It is observed that the distance between the centers of neighboring silica particles is $\sqrt{2}D$, where D is the diameter of templating silica colloids. The ETPTA nanostems, whose sizes and shapes can be adjusted by applying different plasma etching treatments, are seen in the cross-sectional SEM image (Figure 1d). Owing to the formation of covalent bonds between ETPTA polymer nanostems and the APTCS-primed silicon wafer, the nanostems are chemically adhered on the wafer surface.[39,40]

A poly(vinyl alcohol) (PVA) aqueous solution with hydrochloric acid (0.2 vol %) is then casted upon the plasma-etching-treated monolayer colloidal crystal specimen. Because the addition of hydrochloric acid facilitates the formation of covalent bonds through hydroxyl condensation reactions between PVA macromolecules and the hydroxyl groups on silica particles, silica particles are removed as the PVA film is peeled off from the silicon wafer surface after drying.[41] By contrast, the underneath ETPTA nanostems are still anchored on the silicon wafer. In addition, the weak attachment between silica particles and ETPTA polymer promotes effective separation of silica nanocaps from the ETPTA nanostems. Figure 2 confirms that the silica particles are successfully removed from the wafer surface and uniformly embedded in the PVA film. It is clearly observed that the arrangement of silica particles is well retained, leading to the constitution of hexagonal non-close-packed nanohole arrays, which are replicas of the ETPTA nanostems.

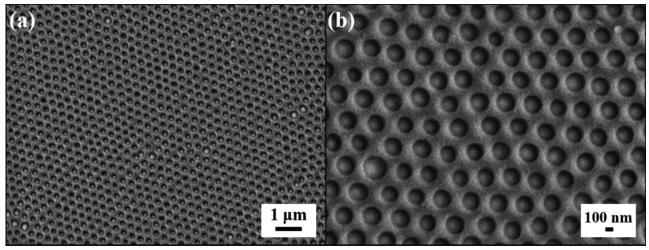

Figure 2. (a) Top-view and (b) side-view SEM images of a PVA composite film with embedded 250 nm silica colloidal crystals.

The templated nanoholes can serve as second-generation templates to develop nanosuckers. Poly(dimethylsiloxane) (PDMS) exhibits numerous advantages coming from its intrinsic properties, such as being deformable, gas permeable, waterproof, biocompatible, nonhemolytic, and nontoxic, and therefore minimizes immune reactions or inflammation on the wounds.[42−46] In this study, a PDMS precursor layer is casted over the PVA template and solidified by a thermal curing process. PDMS nanosucker arrays are then fabricated after peeling off the PVA mold. Figure 3a,b displays the side-view SEM images of the resulting PDMS nanosuckers. The structures with concave surfaces and slanting angle sidewalls are created throughout the soft-lithography-like replication. It is observed that the size of the PDMS nanosuckers are reduced by about 5% more than the size of ETPTA nanostems due to the volume shrinkage of the PVA mold, resulting from the evaporation of entrapped water in the PVA macromolecular network during the solidification of the PDMS precursor. Moreover, it is apparent that long-range hexagonal ordering and the interstructure distance are well retained.

Figure 3c presents the appearance of a 4 in. diameter PDMS nanosucker array templated from a PVA mold consisting of 250

DOI: 10.1021/acsnano.7b00809
ACS Nano 2017, 11, 5332−5338

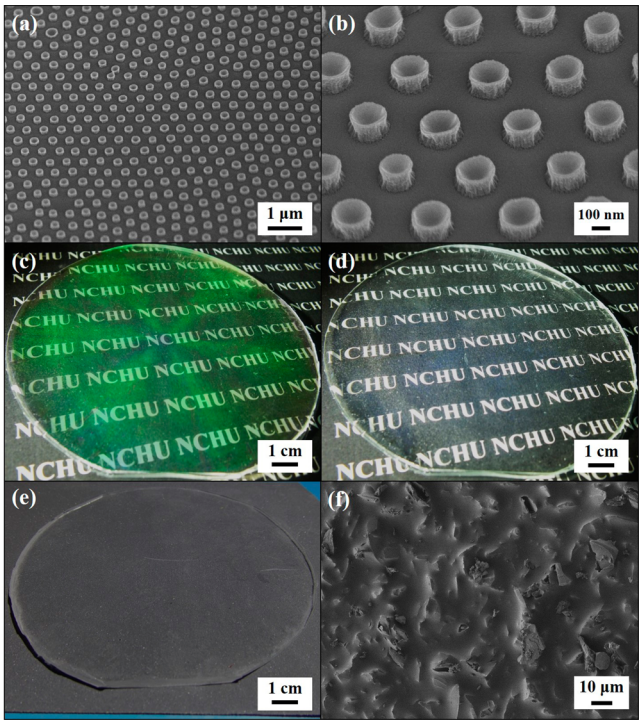

Figure 3. (a) Side-view SEM image of a PDMS nanosucker array templated from a PVA composite film. (b) Magnified side-view SEM image of the same sample as in (a). (c) Photograph of a 4 in. sized PDMS nanosucker array illuminated with white light. (d) Photograph of the same sample as in (c) adhering to a glass substrate. The use of the logo is permitted from National Chung Hsing University. (e) Photograph of the same sample as in (c) adhering to a piece of sandpaper. (f) Top-view SEM image of the sandpaper shown in (e).

nm silica colloidal crystals illuminated with white light. It is clearly evident that a characteristic six-arm pattern on the PDMS film is preserved. The pattern results from Bragg diffraction of visible light from the hexagonal non-close-packed nanosucker array, indicating that the periodic domain ordering over centimeter-size scale can be achieved. As the PDMS film is pressed against a flat glass substrate, the flexible nanosuckers conform to the substrate and deform with release of the internal air between nanosuckers and the substrate, forming a seal and generating an adhesion force. Interestingly, in comparison with an unpressed nanosucker-covered PDMS film, the pressed one is uniformly transparent for a few square centimeters, where the characters underneath the film are clearly visible (Figure 3d). The transparent sample further confirms the deformation of nanosuckers, so that incident light is not diffracted from the sample. This indicates that the adhesion behaviors on substrates can be determined from the appearance of the nanosucker-covered PDMS film.

Importantly, the octopus-inspired nanosuckers are capable of forming seals on uneven surfaces. As shown in Figure 3e, after being pressed, the nanosucker-covered PDMS film is adhered to a piece of sandpaper, whose surface has been fixed with 10 μm scale abrasive grains produced from silicon carbide (Figure 3f). The transparent appearance reveals that nanosuckers on the PDMS film can be deformed and release the air between that and the sandpaper. This further confirms that the as-developed materials can generate an adhesion force on both flat surfaces and microrough surfaces.

Nanosuckers utilize adhesion force derived from van der Waals force and negative pressure effect. The adhesive performance of a blank PDMS film is investigated with a target surface of glass. As can be seen in Figure S1, the unpatterned PDMS film exhibits a normal adhesion force of around 0.05 N per square centimeter, which is induced by the van der Waals force between the PDMS film and the glass surface. The normal adhesion force of a nanosucker array sample on flat substrates can be theoretically estimated by $F_{normal} = \Delta P \times A_{total}$, where ΔP is the pressure differential between the ambient pressure and the pressure inside the nanosucker, and A_{total} is the total area of attachment. Assuming the volume of trapped air between the pressed nanosucker and a flat substrate reaches 0, the $\Delta P = 10.1$ N/cm^2, and the area of attachment for each nanosucker can be estimated using

$$A = \int_0^{2\pi} \int_{-\pi/2}^{\beta-\pi/2} R^2 \cos\varphi \, d\varphi \, d\theta \quad (1)$$

where R is the radius of templating silica colloids. As illustrated in Figure 4, $R \sin\beta = r$ and $r \approx 100$ nm (Figure 3b). The

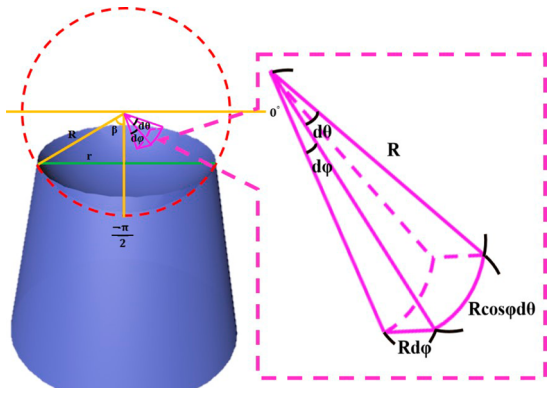

Figure 4. Illustration of a fabricated PDMS nanosucker structure.

calculated β and φ are 53° and 37°, respectively. By substituting the calculated φ into formula 1, it is found that A is equal to 3.9 $\times 10^{-10}$ cm^2. Moreover, as the intersucker distance is $\sqrt{2}D$, the number of nanosuckers on a 1 cm^2 nanosucker-covered PDMS film can be expressed by $N = \left(\frac{1\text{ cm}}{\sqrt{2}D}\right)^2$, where $D = 250$ nm. It is estimated that N equals 8.0 $\times 10^8$, and hence A_{total} equals 0.3 cm^2. Therefore, in the case of a 1 cm^2 PDMS nanosucker array sample, the theoretical adhesion force in the normal direction is approximately equal to 3.2 N, which is much larger than the van der Waals force.

To further comprehend the adhesive capacities of the fabricated nanosucker-covered PDMS film, a tension meter is applied to measure the adhesion forces. For a 1 cm^2 PDMS nanosucker array sample, the average adhesion forces in the normal direction are 3.0 N on dry glass surfaces and 2.8 N on wet glass surfaces (Figure 5a,b), which are competitive among dry polymer-based adhesives.[47−53] In addition, the results reveal that the normal adhesion forces on dry surfaces and wet surfaces are about 94 and 88% of the theoretical value, respectively. This indicates that the water contained in nanosuckers on wet surfaces can sustain negative pressures. During attachment, the nanosucker array not only resists perpendicular forces that incline to lift the nanosuckers from the surface but also resists shearing forces that incline to slide the nanosuckers in the direction parallel to the surface.[54] It is

DOI: 10.1021/acsnano.7b00809
ACS Nano 2017, 11, 5332−5338

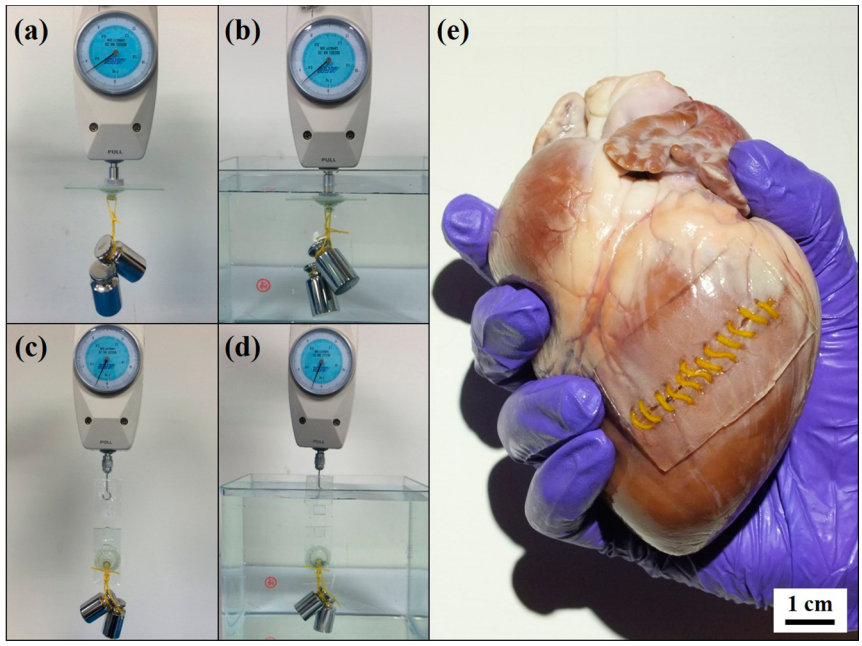

Figure 5. Adhesion force characteristics of a 1 cm^2 PDMS nanosucker array sample performed by a tension meter. Normal adhesion forces (a) under a dry condition and (b) in a wet environment. Shear adhesion forces (c) under a dry condition and (d) in a wet environment. (e) Photograph of a 10 cm^2 PDMS nanosucker array sample adhering to a porcine (pig) heart.

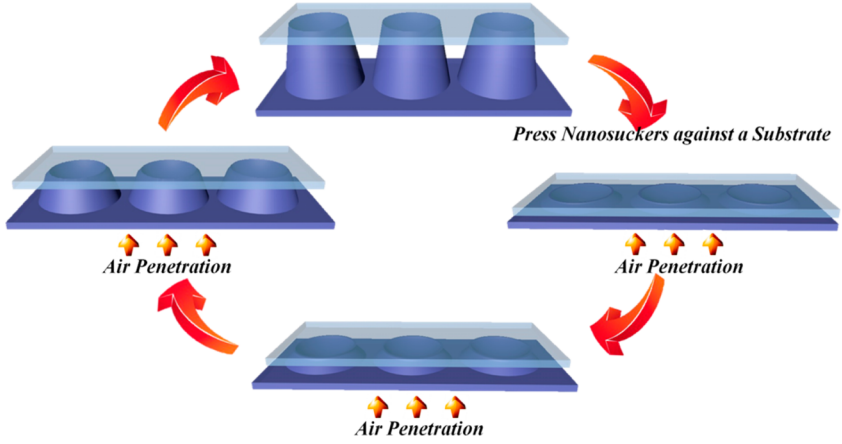

Figure 6. Schematic illustration of the attachment and detachment mechanisms.

observed that the average shear adhesion forces on dry glass surfaces and wet glass surfaces are 1.3 and 1.2 N, respectively (Figure 5c,d). The theoretical shear adhesion force of the nanosucker array sample on flat substrates can be calculated by $F_{shear} = F_{normal} \times \mu$, where the friction coefficient between PDMS and glass substrate (μ) is around 0.5.[55,56] The theoretical shear adhesion force equals 1.6 N, which is close to the measured values. Importantly, by reducing the size of the suckers, the thickness of the water film confined between the nanosuckers and a wet surface reduces faster by applying the same pressing pressure. As a consequence, the water film in the contact region becomes thinner, leading to the increase of friction coefficient. As the nanosucker array is attached to an object, any force tends to remove the nanosuckers from the surface, resulting in further decrease of pressure inside the sucker.

It is significant to note that the nanosucker adhesion is maintained over multiple contact cycles on both wet and dry surfaces. The schematic illustration of the attachment and detachment mechanisms is displayed in Figure 6. As the nanosuckers are pressed against a substrate, the flexible nanosuckers confirm to the substrate and deform by releasing the internal air between nanosuckers and the substrate, forming a seal and generating an adhesion force. With high silicon–oxygen chain flexibility, great rotational mobility and large free volume, PDMS is known as one of the most gas-permeable polymers. Under a dry condition, air can permeate across the nanosucker-covered PDMS film in the direction from outside of the film to the space between nanosuckers and the substrate. This causes the decrease of pressure differential between the ambient pressure and the pressure inside the nanosuckers, resulting in the detachment of nanosuckers. For the case of a wet substrate, the sample is dried, while the detachment procedure is performed in the ambient environment. The presence of water provides better sealing and thus takes longer for detachment. As shown in Figure 7, the octopus-inspired adhesion can be repeatedly used for more than 10 times. It is observed that more contact cycles result in lower adhesion,

DOI: 10.1021/acsnano.7b00809
ACS Nano 2017, 11, 5332–5338

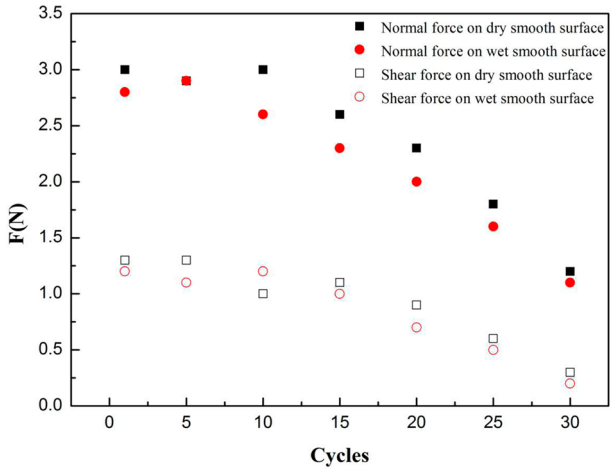

Figure 7. Adhesion force characteristics of a 1 cm^2 PDMS nanosucker array sample under a dry condition and in a wet environment.

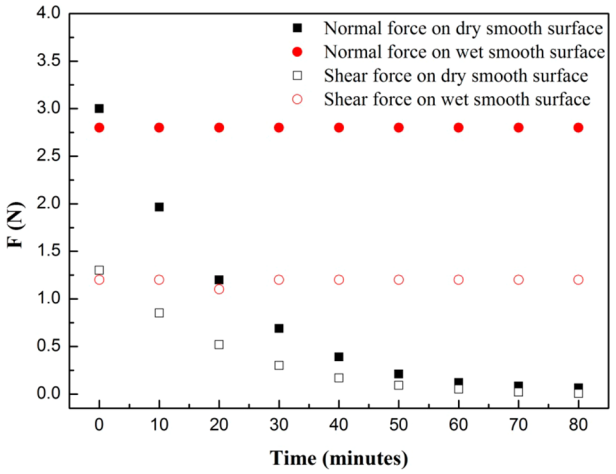

Figure 9. Adhesion strength of a 1 cm^2 nanosucker-covered PDMS film under a dry condition and in a wet environment as a function of the time of attachment.

which is caused by the deformation of flexible nanosuckers in the attachment procedure (Figure 8).

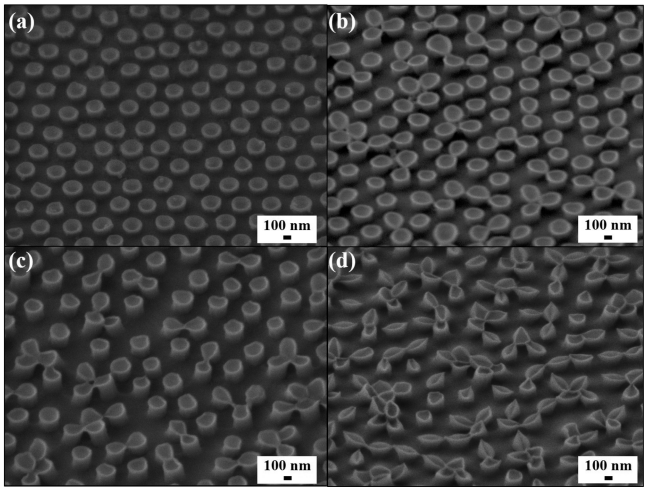

Figure 8. Side-view SEM image of a PDMS nanosucker array performed in the attachment and detachment procedure for (a) one cycle, (b) 10 cycles, (c) 20 cycles, and (d) 30 cycles.

In order to comprehend the adhesion performance of the nanosucker-covered PDMS film, the time-dependent variation of adhesion strength in the ambient environment is evaluated (Figure 9). It is notable that the adhesion strength of nanosuckers on a dry glass surface gradually decreases over time. This can be explained by air permeation characteristics for the nanosucker-covered PDMS film, as displayed in Figure S2. In the early stage, the pressure at the permeation side of the PDMS film increases linearly, resulting in the decrease of pressure differential. This leads to the decrease of adhesion force under a dry condition. After 60 min, the normal adhesion force and shear adhesion force on a dry surface approximately reach 0 N, resulting from the low pressure differential. Importantly, the octopus-inspired nanosucker arrays do not require a preload during the detaching process, which are promising for a variety of technological applications such as temporary gauze materials. Although further testing is required, it is expected that the long-term adhesions can be achieved using non-gas-permeable flexible materials to replace PDMS. In comparison to that, the octopus-inspired adhesion can be maintained longer than 80 min in water, demonstrating the adhesion performance in wet environments.

To gain a better understanding of the adjustable adhesion, the monolayer non-close-packed colloidal crystals consisting of 250 nm silica particles (Figure 1b) are used as etching masks during an argon RIE treatment, followed by a wet-etching procedure to pattern nanosucker arrays (Figure S3). By comparing Figure 1b and Figure S3, it is evidenced that the long-range hexagonal ordering and interstructure distance are preserved. It is also observed that $r \approx 150$ nm and the interstructure distance is $\sqrt{2}D$, where $D = 250$ nm. For 1 cm^2 PDMS nanosucker arrays, the average adhesion forces in the normal direction and in the shear direction on dry glass surfaces can reach 6.9 and 3.5 N, respectively, whereas the theoretical normal adhesion force equals 7.2 N and the theoretical shear adhesion force equals 3.6 N, which are close to the experimental values. The results further demonstrate that the structure of the nanosuckers also affects the adhesive capacities. As a proof-of-concept application, once the nanosucker array is pressed against a porcine heart, the nanosuckers can generate an adhesion force (Figure 5e). It is worth mentioning that the optically clear film dressings allow readily and easy inspection on wound healing progress and any drainage for optimal healing.

CONCLUSIONS

In summary, an uncomplicated and scalable templating technology for fabricating non-close-packed nanosuckers on PDMS substrates has been developed. The templated nanosucker arrays exhibit great adhesive capacities on both dry surfaces and wet surfaces. In addition, resulting from the good flexibility of the PDMS, the nanosuckers can be deformed and generate an adhesion force on microrough surfaces. The technology is compatible with standard industrial manufacturing and provides a platform for varieties of medical applications ranging from hemostasis, wound care, and wound nursing.

EXPERIMENTAL SECTION

Fabrication of Non-close-Packed Monolayer Colloidal Crystals. The preparation of monolayer non-close-packed silica

DOI: 10.1021/acsnano.7b00809
ACS Nano 2017, 11, 5332−5338

colloidal crystals was performed following the well-established spin-coating procedures.[57,58] Monodispersed silica colloids with 250 nm diameter were synthesized according to the Stöber method.[59] The silica colloids were purified in 200 proof ethanol (Echo Chemicals) by multiple centrifugation/redispersion cycles and then redispersed in UV-curable ethoxylated trimethylolpropane triacrylate monomer (SR 454, Sartomer) with 1 vol % 2-hydroxy-2-methyl-1-phenyl-1-propanone (Darocur 1173, BASF) as the photoinitiator. The final silica colloid volume fraction was adjusted to be *ca.* 20 vol %. After filtration through a 5 μm syringe filter (Whatman) to remove any particle aggregates, the silica colloidal suspension was dispersed on a silicon wafer (n-type, Wafernet), which was primed by 3-acryloxypropyl trichlorosilane (APTCS) and then coated by a polymerized ETPTA wetting layer before use. The ETPTA wetting-layer-coated silicon wafer was tilted and rotated to spread the suspension and was then spun at 1000 rpm for 20 s, 3000 rpm for 20 s, 6000 rpm for 20 s, and 8000 rpm for 180 s using a spin coater (WS-400B-6NPP-Lite spin process, Laurell). The ETPTA monomer was then photopolymerized by exposure to UV radiation for 10 s using a pulsed UV curing system (X Lite 500, OPAS).

Reactive Ion Etching. Oxygen and argon RIE was performed on a Unaxis Shuttlelock RIE/ICP reactive ion etcher. To release the embedded silica particles, oxygen RIE operating at 40 mTorr chamber pressure, 20 sccm oxygen flow rate, and 100 W was carried out for 60 s. The monolayer silica colloidal crystals were then used as etching masks during an oxygen/argon RIE treatment (40 mTorr chamber pressure, 20 sccm oxygen flow rate and 20 sccm argon flow rate, and 100 W) and an argon RIE process (40 mTorr chamber pressure, 40 sccm argon flow rate, and 100 W) to pattern mushroom-like structure arrays directly on the silicon wafer.

Soft-Lithography-like Replication. A 10 vol % poly(vinyl alcohol) (Sigma-Aldrich) aqueous solution with 0.2 vol % hydrochloric acid (Sigma-Aldrich) was poured onto the oxygen/argon plasma-treated monolayer colloidal crystal sample. After being dried at room temperature, the PVA film was peeled off from the silicon wafer surface. Poly(dimethylsiloxane) (Sylgard 184, Dow Corning) precursors were mixed and degassed, followed by pouring over the as-fabricated silica colloidal crystal/PVA composite film. After being cured at 70 °C for 1 h, the solidified PDMS film was peeled off from the PVA film.

Air Permeation Measurement. The tested specimen was placed on the porous steel which was covered by a filtration paper. Constant pressure of air was maintained at the feed side, and vacuum was set at the permeation side at the beginning of the experiment. Increase of pressure at the permeation side with time was measured at room temperature using a pressure transducer to evaluate the air permeability.

Characterization. Field-emission scanning electron microscopy was performed on a JEOL 6335F FEG-SEM. A thin layer of gold was sputtered onto the specimens prior to imaging. A digital camera (Nikon Coolpix L810) was employed to acquire images of the specimens. Adhesion force characteristics of the samples were conducted using a tension meter (NK-20). The specimens were pressed against dry or wet glass surfaces and then peeled off in the normal direction and in the shear direction. The experimental measurement was repeated five times for each specimen, and the average of these measurements was reported.

ASSOCIATED CONTENT

Supporting Information

The Supporting Information is available free of charge on the ACS Publications website at DOI: 10.1021/acsnano.7b00809.

Photograph of a blank PDMS film adhering to a glass substrate; experimental permeation characteristics for a nanosucker-covered PDMS film; SEM images of a PDMS nanosucker array fabricated by applying an argon RIE process (PDF)

AUTHOR INFORMATION

Corresponding Author

*E-mail: hyang@dragon.nchu.edu.tw.

ORCID

Hongta Yang: 0000-0002-5822-1469

Notes

The authors declare no competing financial interest.

ACKNOWLEDGMENTS

Acknowledgment is made to Ministry of Science and Technology (Grant Nos. MOST 104-2221-E-005-086 and MOST 105-2221-E-005-090) for support of this research.

REFERENCES

(1) Ramakrishna, S.; Mayer, J.; Wintermantel, E.; Leong, K. W. Biomedical Applications of Polymer-Composite Materials: A Review. *Compos. Sci. Technol.* **2001**, *61*, 1189−1224.

(2) Gist, S.; Tio-Matos, I.; Falzgraf, S.; Cameron, S.; Beebe, M. Wound Care in the Geriatric Client. *Clin. Interventions Aging* **2009**, *4*, 269−287.

(3) Wang, L. S.; Chow, P. Y.; Tan, D. C. W.; Zhang, W. D.; Yang, Y. Y. Nanostructured and Transparent Polymer Membranes with Thermosensitivity for Wound Dressing and Cell Grafting. *Adv. Mater.* **2004**, *16*, 1790−1794.

(4) Villarreal-Gomez, L. J.; Vera-Graziano, R.; Vega-Rios, M. R.; Pineda-Camacho, J. L.; Mier-Maldonado, P. A.; Almanza-Reyes, H.; Cornejo Bravo, J. M. *In vivo* Biocompatibility of Dental Scaffolds for Tissue Regeneration. *Adv. Mater. Res.* **2014**, *976*, 191−195.

(5) Lloyd, J. D., 3rd; Marque, M. J.; Kacprowicz, R. F. Closure Techniques. *Emerg. Med. Clin. North Am.* **2007**, *25*, 73−81.

(6) Ito, T.; Akutsu, T.; Saito, T.; Numata, T.; Tokumura, F.; Kusumi, K.; Ohyama, K. Adhesive Material for Hemostasis and a Method for Hemostasis. U.S. Patent 5690610, 1997.

(7) Lee, K. H.; Tong, T. G. Mechanism of Action of Retinyl Compounds on Wound Healing II: Effect of Active Retinyl Derivatives on Granuloma Formation. *J. Pharm. Sci.* **1970**, *59*, 1195−1197.

(8) Duarte, A. P.; Coelho, J. F.; Bordado, J. C.; Cidade, M. T. T.; Gil, M. H. Surgical Adhesives: Systematic Review of the Main Types and Development Forecast. *Prog. Polym. Sci.* **2012**, *37*, 1031−1050.

(9) Giano, M. C.; Ibrahim, Z.; Medina, S. H.; Sarhane, K. A.; Christensen, J. M.; Yamada, Y.; Brandacher, G.; Schneider, J. P. Injectable Bioadhesive Hydrogels with Innate Antibacterial Properties. *Nat. Commun.* **2014**, *5*, 4095.

(10) Yang, S. Y.; O'Cearbhaill, E. D.; Sisk, G. C.; Park, K. M.; Cho, W. K.; Villiger, M.; Bouma, B. E.; Pomahac, B.; Karp, J. M. A Bio-Inspired Swellable Microneedle Adhesive for Mechanical Interlocking with Tissue. *Nat. Commun.* **2013**, *4*, 1702.

(11) Bouten, P. J. M.; Zonjee, M.; Bender, J.; Yauw, S. T. K.; van Goor, H.; van Hest, J. C. M.; Hoogenboom, R. The Chemistry of Tissue Adhesive Materials. *Prog. Polym. Sci.* **2014**, *39*, 1375−1405.

(12) Fischer, K. E.; Alemán, B. J.; Tao, S. L.; Daniels, R. H.; Li, E. M.; Bünger, M. D.; Nagaraj, G.; Singh, P.; Zettl, A.; Desai, T. A. Biomimetic Nanowire Coatings for Next Generation Adhesive Drug Delivery Systems. *Nano Lett.* **2009**, *9*, 716−720.

(13) Ye, K.; Wang, X.; Cao, L.; Li, S.; Li, Z.; Yu, L.; Ding, J. Matrix Stiffness and Nanoscale Spatial Organization of Cell-Adhesive Ligands Direct Stem Cell Fate. *Nano Lett.* **2015**, *15*, 4720−4729.

(14) Spotnitz, W. D.; Burks, S. Hemostats, Sealants, and Adhesives: Components of the Surgical Toolbox. *Transfusion* **2008**, *48*, 1502−1516.

(15) Spotnitz, W. D.; Burks, S. Hemostats, Sealants, and Adhesives II: Update As Well As How and When to Use the Components of the Surgical Toolbox. *Clin. Appl. Thromb./Hemostasis* **2010**, *16*, 497−514.

(16) Zaleski, G. X.; Funaki, B.; Gentile, L.; Garofalo, R. S. Purse-String Sutures and Miniature Tourniquet to Achieve Immediate Hemostasis of Percutaneous Grafts and Fistulas: A Simple Trick with a Twist. *AJR, Am. J. Roentgenol.* **2000**, *175*, 1643−1645.

DOI: 10.1021/acsnano.7b00809
ACS Nano 2017, 11, 5332−5338

(17) Kweon, D. K.; Song, S. B.; Park, Y. Y. Preparation of Water-Soluble Chitosan/Heparin Complex and Its Application as Wound Healing Accelerator. *Biomaterials* **2003**, *24*, 1595−1601.
(18) Vournakis, J. N.; Demcheva, M.; Whitson, A. B.; Finkielsztein, S.; Connolly, R. J. The RDH Bandage: Hemostasis and Survival in A Lethal Aortotomy Hemorrhage Model. *J. Surg. Res.* **2003**, *113*, 1−5.
(19) Srinivasarao, M. Nano-Optics in the Biological World: Beetles, Butterflies, Birds, and Moths. *Chem. Rev.* **1999**, *99*, 1935−1962.
(20) Bußhardt, P.; Kunze, D.; Gorb, S. N. Interlocking-Based Attachment During Locomotion in the Beetle Pachnoda marginata (Coleoptera, Scarabaeidae). *Sci. Rep.* **2015**, *4*, 6998.
(21) Spinner, M.; Westhoff, G.; Gorb, S. N. Subdigital Setae of Chameleon Feet: Friction-Enhancing Microstructures for a Wide Range of Substrate Roughness. *Sci. Rep.* **2015**, *4*, 5481.
(22) Yu, J.; Chary, S.; Das, S.; Tamelier, J.; Pesika, N. S.; Turner, K. L.; Israelachvili, J. N. Gecko-Inspired Dry Adhesive for Robotic Applications. *Adv. Funct. Mater.* **2011**, *21*, 3010−3018.
(23) Tramacere, F.; Beccai, L.; Kuba, M.; Gozzi, A.; Bifone, A.; Mazzolai, B. The Morphology and Adhesion Mechanism of Octopus Vulgaris Suckers. *PLoS One* **2013**, *8*, e65074.
(24) Kier, W. M.; Smith, A. M. The Structure and Adhesive Mechanism of Octopus Suckers. *Integr. Comp. Biol.* **2002**, *42*, 1146−1153.
(25) Hou, J.; Wright, E.; Bonser, R. H. C.; Jeronimidis, G. Development of Biomimetic Squid-Inspired Suckers. *J. Bionic Eng.* **2012**, *9*, 484−493.
(26) Varenberg, M.; Gorb, S. N. Hexagonal Surface Micropattern for Dry and Wet Friction. *Adv. Mater.* **2009**, *21*, 483−486.
(27) Wainwright, D. K.; Kleinteich, T.; Kleinteich, A.; Gorb, S. N. A. P.; Summers, A. P. Stick Tight: Suction Adhesion on Irregular Surfaces in the Northern Clingfish. *Biol. Lett.* **2013**, *9*, 20130234.
(28) Chang, W. Y.; Wu, Y.; Chung, Y. C. Facile Fabrication of Ordered Nanostructures from Protruding Nanoballs to Recessional Nanosuckers *via* Solvent Treatment on Covered Nanosphere Assembled Monolayers. *Nano Lett.* **2014**, *14*, 1546−1550.
(29) Follador, M.; Tramacere, F.; Mazzolai, B. Dielectric Elastomer Actuators for Octopus Inspired Suction Cups. *Bioinspiration Biomimeticsi* **2014**, *9*, 046002.
(30) Xue, L.; Kovalev, A.; Dening, K.; Eichler-Volf, A.; Eickmeier, H.; Haase, M.; Enke, D.; Steinhart, M.; Gorb, S. N. Reversible Adhesion Switching of Porous Fibrillar Adhesive Pads by Humidity. *Nano Lett.* **2013**, *13*, 5541−5548.
(31) Choi, M. K.; Park, O. K.; Choi, C.; Qiao, S.; Ghaffari, R.; Kim, J.; Lee, D. J.; Kim, M.; Hyun, W.; Kim, S. J.; Hwang, H. J.; Kwon, S. H.; Hyeon, T.; Lu, N.; Kim, D. H. Cephalopod-Inspired Miniaturized Suction Cups for Smart Medical Skin. *Adv. Healthcare Mater.* **2016**, *5*, 80−87.
(32) Lee, H.; Um, D. S.; Lee, Y.; Lim, S.; Kim, H. J.; Ko, H. Octopus-Inspired Smart Adhesive Pads for Transfer Printing of Semiconducting Nanomembranes. *Adv. Mater.* **2016**, *28*, 7457−7465.
(33) Chu, B.; Jung, K.; Han, C. S.; Hong, D. A Survey of Climbing Robots: Locomotion and Adhesion. *Int. J. Precis. Eng. Man.* **2010**, *11*, 633−647.
(34) Min, W. L.; Jiang, B.; Jiang, P. Bioinspired Self-Cleaning Antireflection Coatings. *Adv. Mater.* **2008**, *20*, 3914−3918.
(35) Chen, Y. C.; Huang, Z. S.; Yang, H. Cicada Wing Inspired Self-Cleaning Antireflection Coatings on Polymer Substrates. *ACS Appl. Mater. Interfaces* **2015**, *7*, 25495−25505.
(36) Isa, L.; Kumar, K.; Muller, M.; Grolig, J.; Textor, M.; Reimhult, E. Particle Lithography from Colloidal Self-Assembly at Liquid−Liquid Interfaces. *ACS Nano* **2010**, *4*, 5665−5670.
(37) Jiang, P.; McFarland, M. J. Wafer-Scale Periodic Nanohole Arrays Templated from Two-Dimensional Nonclose Packed Colloidal Crystals. *J. Am. Chem. Soc.* **2005**, *127*, 3710−3711.
(38) Sun, C. H.; Jiang, P.; Jiang, B. Broadband Moth-Eye Antireflection Coatings on Silicon. *Appl. Phys. Lett.* **2008**, *92*, 061112.
(39) Yang, H.; Gozubenli, N.; Fang, Y.; Jiang, P. Generalized Fabrication of Monolayer Nonclose Packed Colloidal Crystals with Tunable Lattice Spacing. *Langmuir* **2013**, *29*, 7674−7681.
(40) Iler, R. K. *The Chemistry of Silica*; John Wiley& Sons: New York, 1979.
(41) Belanger, M. C.; Marois, Y. Hemocompatibility, Biocompatibility, Inflammatory and *in vivo* Studies of Primary Reference Materials Low Density Polyethylene and Polydimethylsiloxane: A Review. *J. Biomed. Mater. Res.* **2001**, *58*, 467−477.
(42) Hua, F.; Sun, Y.; Gaur, A.; Meitl, M. A.; Bilhaut, L.; Rotkina, L.; Wang, J.; Geil, P.; Shim, M.; Rogers, J. A.; et al. Polymer Imprint Lithography with Molecular-Scale Resolution. *Nano Lett.* **2004**, *4*, 2467−2471.
(43) Paguirigan, A. L.; Beebe, D. M. From the Cellular Perspective: Exploring Differences in the Cellular Baseline in Macroscale and Microfluidic Cultures. *Integr. Biol.* **2009**, *1*, 182−195.
(44) Jeong, H. E.; Suh, K. Y. Nanohairs and Nanotubes: Efficient Structural Elements for Gecko-Inspired Artificial Dry Adhesives. *Nano Today* **2009**, *4*, 335−346.
(45) Yoon, H.; Jeong, H. E.; Kim, T. I.; Kang, T. J.; Tahk, D.; Char, K.; Suh, K. Y. Adhesion Hysteresis of Janus Nanopillars Fabricated by Nanomolding and Oblique Metal Deposition. *Nano Today* **2009**, *4*, 385−392.
(46) Ho, A. Y. Y.; Yeo, L. P.; Lam, Y. C.; Rodríguez, I. Fabrication and Analysis of Gecko-Inspired Hierarchical Polymer Nanosetae. *ACS Nano* **2011**, *5*, 1897−1906.
(47) Geim, A. K.; Dubonos, S. V.; Grigorieva, I. V.; Novoselov, K. S.; Zhukov, A. A.; Shapoval, S. Y. Microfabricated Adhesive Mimicking Gecko Foot-Hair. *Nat. Mater.* **2003**, *2*, 461−463.
(48) Federle, W.; Barnes, W. J. P.; Baumgartner, W.; Drechsler, P.; Smith, J. M. Wet but not Slippery: Boundary Friction in Tree Frog Adhesive Toe Pads. *J. R. Soc., Interface* **2006**, *3*, 689−697.
(49) Zhou, M.; Pesika, N.; Zeng, H.; Tian, Y.; Israelachvili, J. Recent Advances in Gecko Adhesion and Friction Mechanisms and Development of Gecko-Inspired Dry Adhesive Surfaces. *Friction* **2013**, *1*, 114−129.
(50) Chary, S.; Tamelier, J.; Turner, K. A Microfabricated Gecko-Inspired Controllable and Reusable Dry Adhesive. *Smart Mater. Struct.* **2013**, *22*, 025013.
(51) Hu, S.; Xia, Z.; Dai, L. Advanced Gecko-Foot-Mimetic Dry Adhesives Based on Carbon Nanotubes. *Nanoscale* **2013**, *5*, 475−486.
(52) Eisenhaure, J. D.; Xie, T.; Varghese, S.; Kim, S. Microstructured Shape Memory Polymer Surfaces with Reversible Dry Adhesion. *ACS Appl. Mater. Interfaces* **2013**, *5*, 7714−7717.
(53) Rahmawan, Y.; Kim, T.; Kim, S. J.; Lee, K. R.; Moon, M. W.; Suh, K. Y. Surface Energy Tunable Nanohairy Dry Adhesive by Broad Ion Beam Irradiation. *Soft Matter* **2012**, *8*, 1673−1680.
(54) Nixon, M.; Dilly, P. N. Sucker Surfaces and Prey Capture. *Symp. Zool.Soc. London* **1977**, *38*, 447−511.
(55) Wang, D.; Möhwald, H. Template-Directed Colloidal Self-Assembly − The Route to 'Top-Down' Nanochemical Engineering. *J. Mater. Chem.* **2004**, *14*, 459−468.
(56) Kier, W. M.; Smith, A. M. The Morphology and Mechanics of Octopus Suckers. *Biol. Bull.* **1990**, *178*, 126−136.
(57) Jiang, P.; Prasad, T.; McFarland, M. J.; Colvin, V. L. Two-Dimensional Nonclose-Packed Colloidal Crystals Formed by Spincoating. *Appl. Phys. Lett.* **2006**, *89*, 011908.
(58) Jiang, P.; McFarland, M. J. Large-Scale Fabrication of Wafer-Size Colloidal Crystals, Macroporous Polymers and Nanocomposites by Spin-Coating. *J. Am. Chem. Soc.* **2004**, *126*, 13778−13786.
(59) Stöber, W.; Fink, A.; Bohn, E. J. Controlled Growth of Monodisperse Silica Spheres in the Micron Size Range. *J. Colloid Interface Sci.* **1968**, *26*, 62−69.

DOI: 10.1021/acsnano.7b00809
ACS Nano 2017, 11, 5332−5338